Characterisation of confinement and impingement effects on the near field of axisymmetric jets using LDA and PIV

by

I. Serres, C. Chauveau, B. Sarh and I. Gökalp

Laboratoire de Combustion et Systèmes Réactifs - CNRS

1C, av. de la Recherche Scientifique - 45071 Orléans cedex 2; France

ABSTRACT

Laser Doppler Anemometry and Particle Image Velocimetry are applied to a domestic burner configuration to determine the effect of geometrical parameters and gas density on the flow field and on the entrainment process. The flow field is that of a confined jet impinging onto a plate. The main design parameters of the experimental devices may be adjusted to modify the confinement ratio and the distance from the outer section of the injector to the stagnation plate. The impinging distance is known to influence the structure of the flow field, mostly when the stagnation plate is in the near field region of the jet. Two density ratios were studied: an isodensity (R_r = 1) and a light jet (R_r = 0.55). The two nominal flow rates were investigated, associated with low Reynolds turbulent jets and laminar jets. A totally transparent new device was manufactured in quartz. This new device presents greater optical accesses for PIV measurements inside the burner. Several configurations were investigated for the different gases and impinging distances: free jets, confined jets, impinging jets, and confined impinging jets (whole burner configurations).

The results concentrate on the jet development and the dynamic field in the vicinity of the stagnation point. The structure of the flow field was investigated in terms of 2D dynamic fields, axial and radial profiles of velocity. A new derivation method for intercorrelation (Hart) is compared with classic FFT intercorrelation, bringing better resolution in the zones of highest velocity gradients. To guarantee high accuracy of the measurements for the whole flow field, two sets of experiments had to be conducted, with two different PIV pulse delay values: one to match the higher velocities encountered in the jet part and the other the lower velocities encountered in the entrainment part. The flow field consists in a combination of these two sets of experiments. The radial jets profiles allow to deduce the entrained air flow rate, against the distance of the stagnation plate as a function of the density ratio. The amount of air entrained by the jet is linked to the density ratio, the length of jet development and also to the pressure gradient due to the impact on the plate. An analysis of the mixture fraction distribution using planar LIF images is in progress.

1. INTRODUCTION

The design process for atmospheric induction burners of gas burning stoves relies today mostly on empirical knowledge gained from experience with prototypes. To meet today's increasingly environmental concerns such as pollutant formation and gain in energy efficiency, a detailed understanding of the mixing processes and of the main characteristics of the dynamic field inside the burner is necessary. Although the experimental facilities are manufactured so as to perform LDA and PIV measurements, their designs are as close as possible to the real burner configuration.

The flow field is that of a variable density confined jet impinging onto a plate. The main design parameters of the experimental devices may be adjusted to modify the confinement ratio and also the distance from the outer section of the injector to the stagnation plate. The impinging distance is known to influence the structure of the flow field, mostly when the stagnation plate is in the near field region of the jet (Baydar, 1999). Two density ratios (1 and 0.55) were studied for two nominal flow rates, associated with low Reynolds turbulent jets and laminar jets. The effect of burner geometry and gas density on the flow field and on the entrainment process is determined.

2. EXPERIMENTAL FACILITIES

Two experimental devices were employed depending on the optical diagnostic used for measurement. One is the industrial burner, slightly modified to allow optical accesses to the jet near-field; the other is a newly simplified burner manufactured in quartz and designed for scientific purposes. This device presents a flexibility to investigate several configurations, from free jet to confined impinging jet, representative of the burner geometry.

2.1 The burner

The device is a partially premixed domestic burner functioning under atmospheric induction: the formation and the homogenisation of the reactive mixture are only due to the entrainment force of the jet issuing from the injector and to the geometrical characteristics of the device (Jones, 1989). The industrial burner (Figure 1) has a power around 3 kW, a 110 mm diameter, and a total height (from the bottom of the basement plate to the burner plate) of about 35 mm. A vertical axisymmetric jet, issuing from an injector fixed on the basement plate, entrains a certain amount of the quiescent surrounding air. The air enters the burner through a small space existing between the supporting plate and the lower burner lip. This entrainment rate depends on the density ratio between the two gases and on the initial momentum of the inductive gas (Ricou and Spalding, 1961). The jet develops in a cylindrical tube, the mixing tube (which has a diameter of 12 times the jet diameter), before impacting onto the plate and spreading inside the mixing chamber. The length of the jet surrounded by the tube is about 8 times the jet diameter. The mixing chamber is characterised by a height fixed around 2.6 mm. The exit of the mixture is realised through slits of three different sizes, alternatively distributed so as to limit flame blow off and flashback. The flames have been checked to be partially premixed laminar flames.

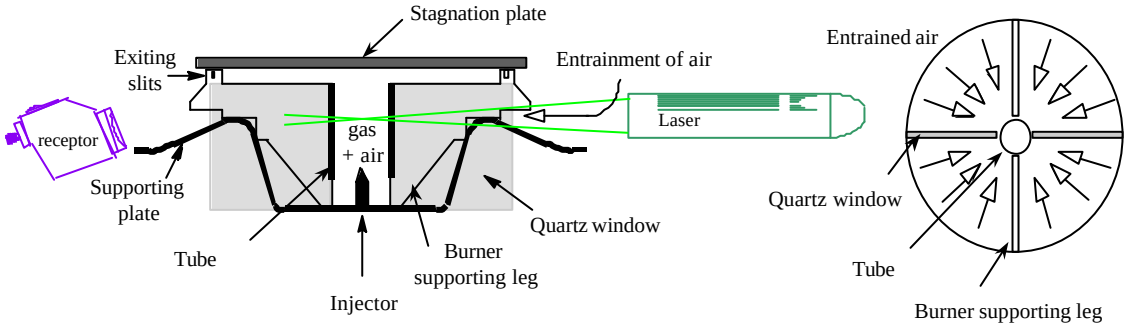

a) Side view section ***b) Schematic above view***

Fig. 1. Experimental set-up for LDA measurements (industrial device).

2.2 The experimental conditions

Two density ratios are studied: an isodensity jet (air jet into air; $R_r = 1$) and a light jet (He/N_2 jet into air; $R_r = 0.55$). The use of inert mixtures instead of reactive gases was entailed to avoid hazards generated by using reactive flow without combustion. Since the injected gases are non reactive, the studies concentrate here on cold flows. The half helium-half nitrogen mixture was chosen in order to match the methane density (0.66 kg/m^3). The density ratio between the surrounding gas and the inducing gas R_r is indeed one of the main parameters governing entrainment in jets (Ricou and Spalding, 1961; Hill, 1972). On the basis of similarity laws for turbulent jets (Pitts, 1991), the injected flow rates were fixed to conserve the initial momentum flux M_j.

$$M_j = 2p \int_0^\infty r\ u^2\, rdr = \frac{p\ r_j\ u_j^2\ D_j^2}{4}$$

Both the full charge and the reduced charge nominal flow rates were investigated. They generate respectively low Reynolds turbulent jets and laminar jets (Table 1).

Tab. 1. Reynolds number and initial momentum flux for the studied jets.

	full charge (high flow rate)			reduced charge (low flow rate)		
M_i (10^{-3} kg.m/s^2)	2.6			0.1		
Re	4300	2500	3500	890	520	710
injected gas	methane	He / N_2	air	methane	He / N_2	air

2.3 The LDA set-up

The Laser Doppler Velocimetry technique is employed to quantify the amount of entrained air through the integration of velocity profiles. The velocimeter is a TSI IFA 755 device, set up in front diffusion. The light source is an Ar-ion laser (green component, 514.5 nm wavelength). A lens with a 242 mm focal length creates an ellipsoidal measurement volume of 0.057 x 0.056 x 0.55 mm^3. The fringe spacing is about 2.5 µm. Oil droplets or smoke particles are the seeding materials, introduced both through the injector (jet seeding) and inside a box surrounding the burner (air seeding). The entrained air is supposed to be initially quiet; any perturbation of it, even slight, involves high uncertainty in the measurements. Taken measurements inside the mixing tube where the disturbances are lower increases the accuracy. To access to this tube two thin planar quartz windows (3.5 mm thick; 45 mm large) have been manufactured directly on the industrial burner, replacing two of the four burner supporting legs (Figure 1).

The use of these windows guarantees the conservation of the measurement volume characteristics (Durst et al., 1981). However the high level of the burner confinement and the thinness of the windows strongly limit both the type of measurements (only the axial component of velocity along a jet diameter is to be obtained) and the investigated zone (only few axial distances are accessible). Furthermore the complexity of the configuration adds major difficulties: the focalisation lens has to be outside the burner, whilst the beam spacing is restricted by the height of the windows and the injector; in the same time the measurement volume formed should be of sufficiently small length in comparison with the jet diameter. This is a critical point since the thin optical accesses imply to align the receptor with the emitting probe (Figure 1). This involves an integration of the velocities of the particles passing through the volume. The influence of this phenomenon is even more important in the jet mixing layers where the velocity gradients are the highest. The choice of the best frequency shifts and filters is quite difficult; the velocity distribution often presents two peaks for which a clear separation is not always possible.

The distance from the injector to the stagnation plate is increased or decreased by rings of various heights or specific stagnation plates (designed to respect the exit surface area). They are inserted above the exiting slits, and the normalised impingement distance H / D varies between 8.8 and 14, where D is the initial jet diameter.

2.4 The PIV apparatus

The dynamic flow field inside the burner is characterised by Particle Image Velocimetry. A totally transparent burner has been designed in quartz to enlarge the zone of measurement up to the stagnation zone. This new facility is simplified and the quartz elements have been optically high polished to reduce the optical reflections. The main change brought to the industrial concept is that the exit ports are replaced by a single slit of equal surface area. Its height has been fixed to 1.1 mm (Figure 2). To vary the confinement ratio on the quartz burner, thin cylinders are set on the basement plate. The exit slit is at the top. This device was also designed to vary the level of geometry complexity from free jets to confined impinging jets.

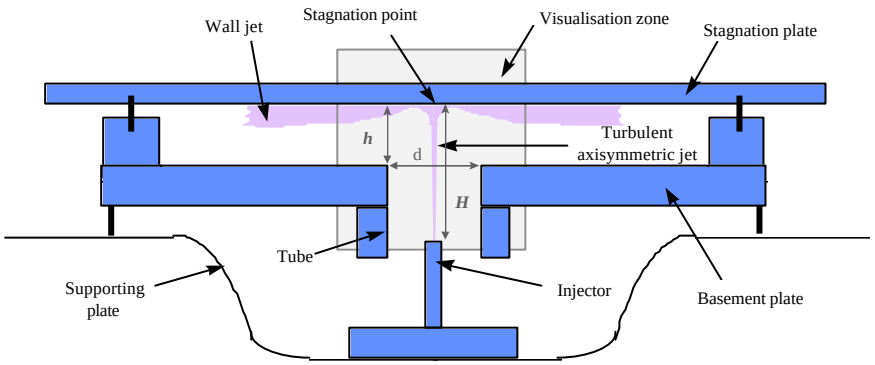

Fig. 2. Experimental PIV set-up: the quartz device.

The PIV system is composed of two 25 mJ Nd:YAG lasers, a lens association creating a thin laser sheet, a high resolution CCD camera, and a software for images acquisition and processing (Insight TSI software). The laser lights the experimental set-up from the top. The decrease in luminous intensity of the laser sheet, due to the beam profile, is uniformly spread out on both sides of the jet axis. The symmetry of the configuration is better conserved than if the laser beam was horizontally oriented. The 22 x 24 mm^2 observation zone focuses on the jet development up to its impingement.

The seeding of the flow is a source of primary difficulties. Both the jet and the entrainment parts should be seeded. The turbulent jets are seeded with oil droplets. The impact on the stagnation plate, combined with the high concentration of droplets, creates a contamination of the surrounding air sufficient to allow the deduction of the velocity vectors. However, the design of the oil injector did not allow to entrain enough seeding for low velocities. Laminar jets involve to use a new seeding technique. Cold smoke particles, passing through a filter to discharge their tar elements, creates a clean seeding, without deposit on the stagnation plate. A drawback of this method is that the entrainment part is not seeded. However laminar jets do not entrain much and the velocities are so small that a specific seeding device will be developed in the future.

As it can be observed on the PIV mean flow fields, the velocity range is wide in a very narrow measurement field, and the velocity gradients are very high in the jet mixing layers. To guarantee high accuracy of the measurements for the whole flow field, two sets of experiments had to be conducted. Two PIV pulse delay values were fixed to match both the higher velocities encountered in the jet part and the lower velocities encountered in the entrainment part. In particular, joined to the high jet velocity (around 60 m/s), the macroscopic $22 \times 24\ mm^2$ visualisation zone involves unusual short pulse delay time (around 2 µs). The velocities of the entrainment part are deduced from a pulse delay time of 100 µs and a pulse delay of 15 µs is adapted to the velocities of the laminar jets.

3. RESULTS AND DISCUSSION

3.1 Effect of the impinging distance on the entrainment

This characterisation is realised from LDA profiles of axial velocity. They are obtained inside the tube of the industrial burner at a fixed section from the injector. Problems of seeding limit the studies to the high flow rate. Mean and fluctuating axial velocity profiles are similar to a coflowing jet. The quantity of air entrained by the jet is deduced from the knowledge of the total mass flow rate integration as followed:

$$\dot{m}_t = 2p \int_0^R r \ \mathrm{U}\, r dr$$

The entrainment rate is obtained by subtracting the injected mass flow rate from the total mass flow rate. For isodensity jets, r is a constant value, while for variable density jets it varies at each location. As a rough approximation, the values for the average density are taken from methane jet literature (same density as the He/N_2 mixture; Pagé, 1998). Planar LIF images recently achieved on the quartz device will improve data accuracy. Figure 3 plots the entrainment rate normalised by the injected mass flow rate for the two density ratios (1 and 0.55), and for the different distances to the stagnation plate.

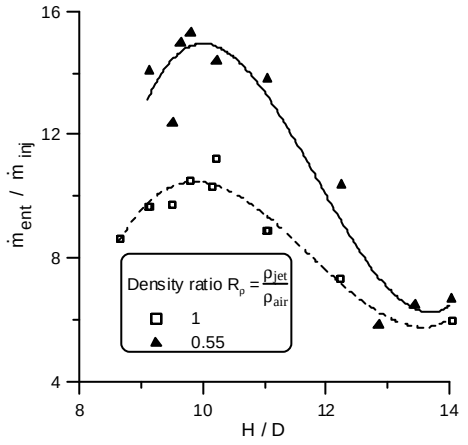

Fig. 3. Effect of the density ratio and of the distance to the stagnation plate on the jet entrainment.

The entrainment force is more efficient for light jets than for isodensity jets. Turbulent confined impinging jets have similar entrainment characteristics than turbulent free jets (Hill, 1972; Djeridane et al., 1996). An optimum of entrainment exists around 10 *D* for both density ratios. It corresponds to the industrial optimised burner design.

3.2 Determination of the dynamic flow field

Figure 4 shows typical tomographic images relative to the burner and the impinging jet cases for the two flow regimes. The plate creates a mirror effect, reflecting the images of the particles inside the quartz thickness, mostly at the impingement point. The seeding contamination for turbulent impinging jets is clearly shown on image *b*. Similar phenomenon occurs also for the burner configuration (image *a*), but intense reflections on the quartz window borders conceal it. Good correlation is not possible and the velocity cannot be deduced at these locations. These parts are masked to avoid generation of spurious vectors in the calculus. The optical reflections are the cause of the blind zones appearing on the dynamic fields (Figure 5). Another source of spurious vectors is the poor correlation due to an inadequate interframe time. As explained in the former paragraph, two dT were applied for two independent sets of measurements, one based on the lower velocities (entrainment part), the other on the higher velocities (jet part). Complementary masks are implemented on the zones where the dT is not adapted. Moreover working with masks guarantees a unique grid for the two sets of experiments.

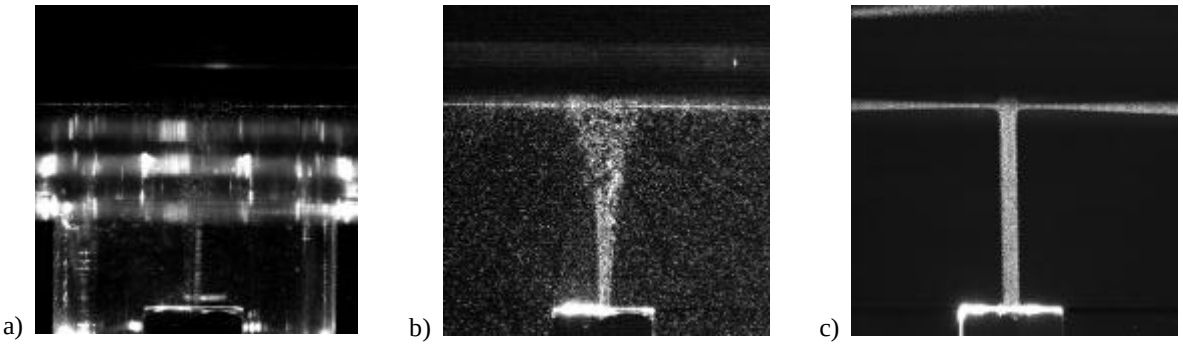

Fig. 4. Examples of tomographic images used for the PIV correlations.
a) low turbulent confined impinging jet (burner configuration)
b) low turbulent impinging jet
c) laminar impinging jet

The images are first intercorrelated by pair using Fast Fourier Transformation performed on small spots representing image parts of 32×32 pixels^2. A 50% overlapping rate generates twice more vectors, i.e. a grid consisting of 61 nodes in the radial direction and 62 in the axial one. The mean field is the result of average on 120 instantaneous fields slightly filtered, using range filter. Then the two sets of experiments conducted with the two PIV pulse delays are combined. Examples of the typical mean flow fields obtained for the different cases of confinement and Reynolds number are shown in Figure 5, as well as an example of unfiltered instantaneous field. The flow fields are well organised: the jet impinges at high velocity, without disturbance until near the plate. From the stagnation point, the flow spreads radially, developing a flow pattern similar to wall jet. At the base of the turbulent jets appears an incompletely developed recirculation zone. For turbulent jets the stream lines of the entrainment are straight and directed towards the stagnation plate; the jet spreading rate is not influenced by the presence of the confinement tube (pictures *b* and *c*). The spreading angle is found around 22°. This value usually characterises turbulent axisymmetric free jets; the jets first develop as free jets.

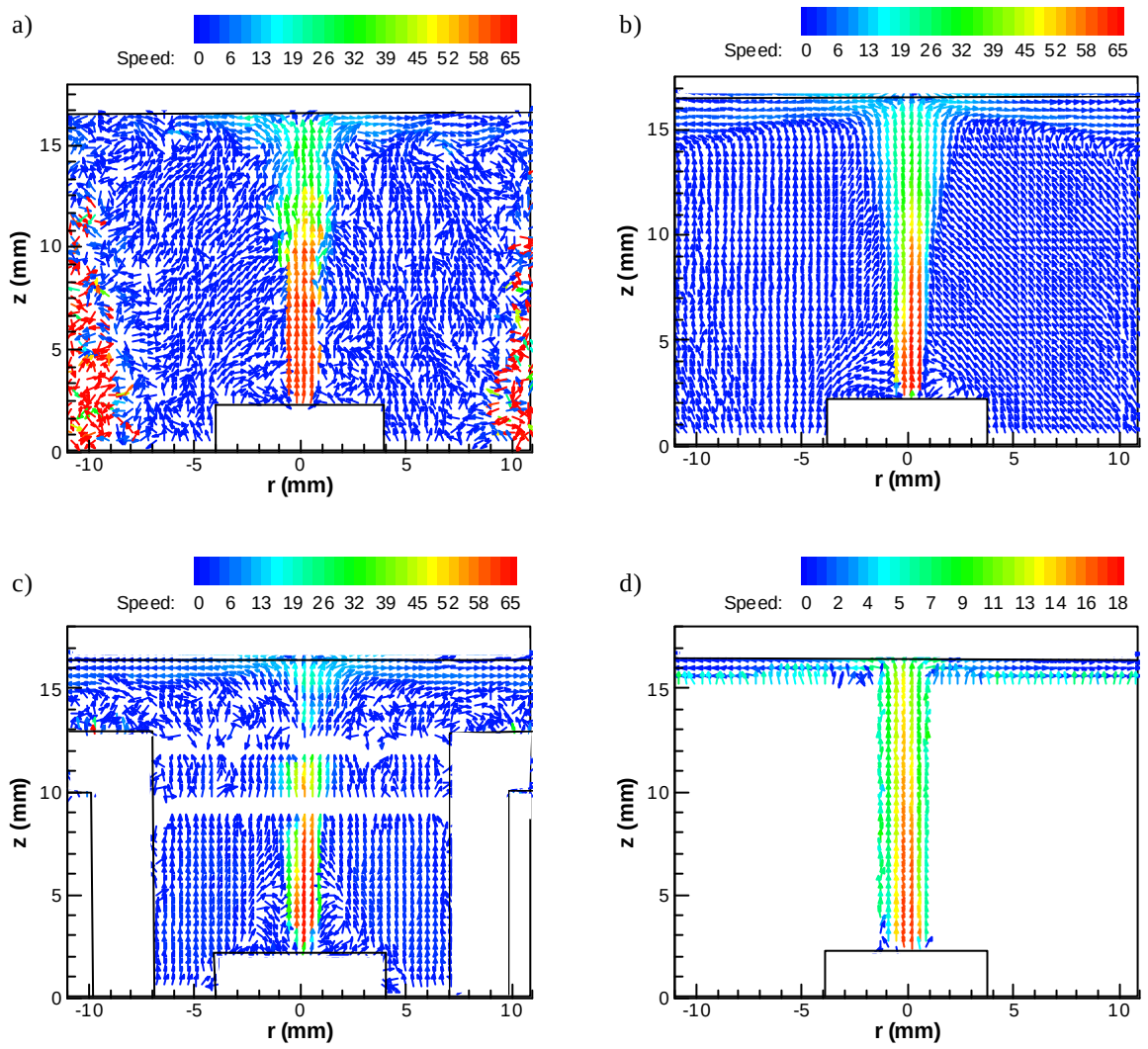

Fig. 5. Typical dynamic fields for the different configurations.
a) instantaneous dynamic field for impinging turbulent jet
b) mean dynamic field for impinging turbulent jet
c) mean dynamic field for confined impinging turbulent jet
d) mean dynamic field for impinging laminar jet

3.3 Comparisons with sparse array image correlation

A comparison between FFT and sparse array image correlations has been performed on the impinging turbulent jet. The latter was devised by Hart (1996) to increase the spatial resolution of the derived dynamic field with reasonable computational time. The method is based on double correlation and sliding interrogation spots. It uses image compression to speed up the process. A compression ratio fixes the threshold for image intensity. The intensity levels lower than this threshold are considered as background noise. A primary window size defines large spots on the images used for a first correlation. A velocity vector is obtained for the whole spot region. The processing spot size will be reduced to secondary defined window size and the corresponding correlation spot on image 2 is shifted based on the amount of the velocity vector calculated. Speed up the process is realised by indicating a maximum search distance in the spot for correlation peaks.

The present investigation was conducted with the Insight TSI software run for the impinging turbulent jet configuration. The compression ratio has been fixed to 95% : only the 5% brightest pixels of the spot is signal. The maximum search distance is of 8 pixels. Two couples of windows and subwindows are investigated: 64 > 32 and 32 > 16. Since a 50% overlap is used, the vectors are twice numerous as the secondary spots size. The interest of running 64 > 32 correlations is to compare FFT and Hart using the same grid. The flow fields are similar. Radial profiles of axial and radial component of velocity have been extracted at z = 10.5 mm and plotted in Figure 6. The representation *rU* (*r*) underlines the entrainment part when the jet is plotted on the same graph, facilitating the comparisons. Plots *a* and *b* are for the *dT* adjusted to the jet part velocities; plots *c* and *d* for the *dT* adjusted to the entrainment part velocities. Although the 2 µs *dT* is not well suited to return accurate velocities in the entrainment part, we compute them. The two methods give the same trends and are different only for the parts where the *dT* are not adapted (entrainment part for *dT* = 2 µs; jet part for *dT* = 100 µs).

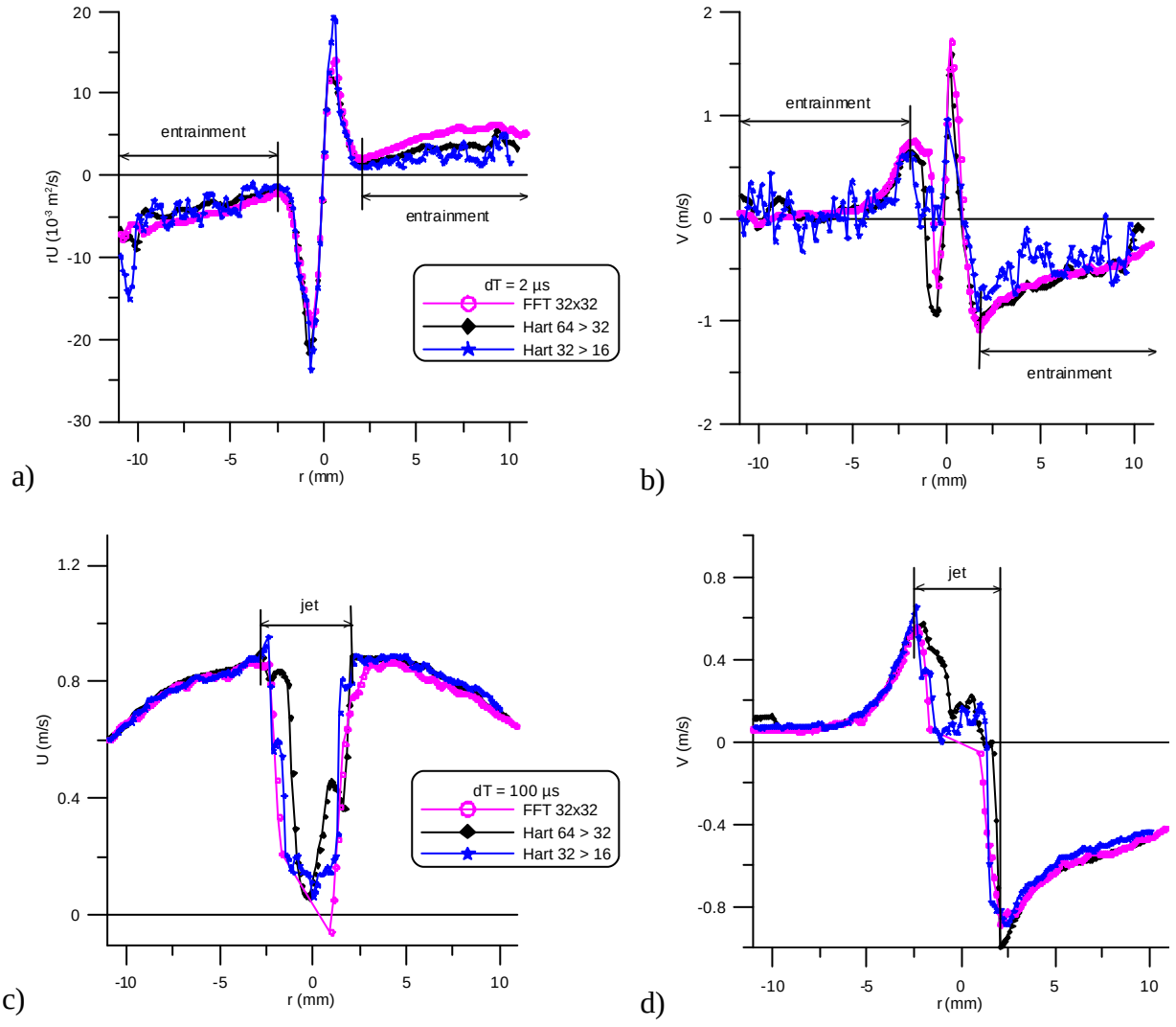

Fig. 6. Comparison between FFT and Hart correlations.

Confident with this new method of correlation, we checked it for smaller windows (32 > 16), which returns a refined mesh. Considering the whole field acquired with the 2 µs pulse delay, we can notice on plots *a* and *b* that the data derived by FFT are less scattered than that derived by the 32 > 16 Hart correlation processing. It evidences that better resolution is driven by the latter method. The FFT correlation appears like an average of the data on bigger spots; Hart correlation is more accurate since the entrainment is not a high stable process (random variations of the seeding, high sensibility to surrounding draughts). When the time delay is well adapted this randomness is smoothed as shown in plots *c* and *d*.

4. IN PROGRESS LIF EXPERIMENTS

Some planar LIF experiments were conducted to estimate the mixture fraction in configurations identical to PIV ones. The final objective is to spatially correlate the data with the dynamic fields obtained in PIV, so as to refine the calculation of the entrained mass flow rate for the variable density jets. Below is presented a synopsis of the approach.

The jet is seeded with about 5 to 10% of diacetyl vapours obtained through a thermostatic bath. A tripled Nd:Yag laser delivers a 355 nm ultra-violet beam capable of exciting the diacetyl particles that emit light in the 430-480 nm wavelength range. A cooled intensified CCD camera records the light intensity as 16 bits 512 x 512 pixels^2 images. The luminous signal is lost in the noise. The background intensity is around 450, the signal around 900, whereas "reflections" on the quartz elements reach 65000. To improve data 600 images were recorded per experiment, as well as 600 images just running the laser without diacetyl (background and "reflections"). This number is a compromise between an optimal dynamic for the mean intensity profiles and the size of the records. The mean image without diacetyl is subtracted from that with diacetyl. Some pixels are negative; they all correspond to "reflections" and so have been forced to zero. In the same way, pixels which intensities are higher than the maximum intensity of the jet zone (where the proportion of diacetyl is the most important) correspond also to "reflections" and are also forced to zero. Figure 7 presents two examples of the images obtained at this stage of the processing. The maximum of the jet zone is used to normalise the mean differential image. The normalised image gives an idea of the mean mixture fraction, as the intensity level is function of the proportion of diacetyl. The diacetyl is a tracer of the gas issuing from the injector. Assuming the proportionality between emitted intensity and mixture fraction, allows to deduce a rough value for the mixture density at each point. After having settled the mesh grids for PIV and LIF measurements, an estimation of the $r\,U$ value at each node is computed.

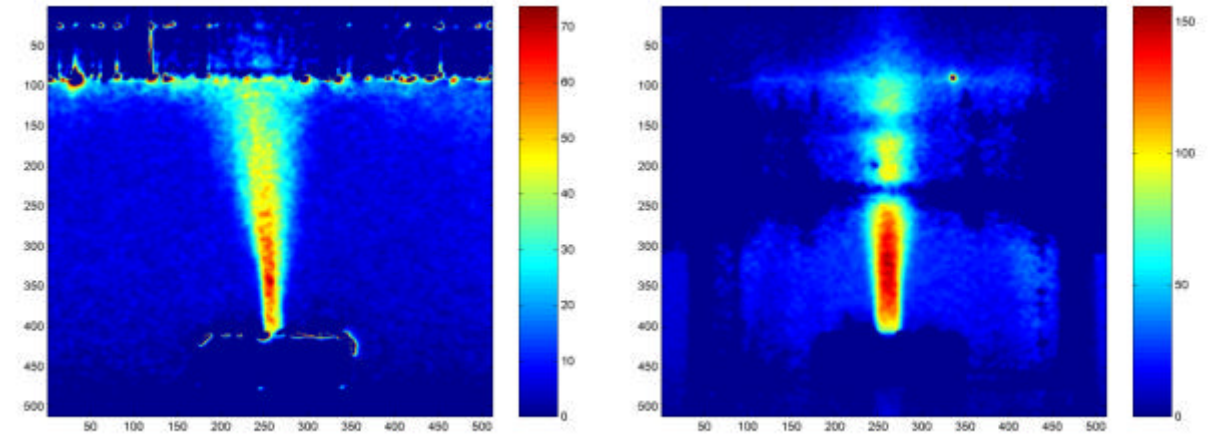

a) b)

Fig. 7. Examples of rescaled intensity images obtained by planar LIF technique.
a) impinging turbulent jet
b) confined impinging turbulent jet

5. CONCLUSION

Fluid Mechanical research optical techniques (LDA and PIV) have been applied to a domestic burner like configuration. The flow field is that of a confined impinging jet either turbulent or laminar depending on the flow rate issuing from the injector. The actual burner was used for the LDA measurements. Thin quartz windows are designed to let the laser beams enter the burner. The accessible profiles are limited to a very restricted zone (axial velocity along a diameter of the jet, inside the tube). Several heights of the stagnation plate were studied in terms of entrainment efficiency. The same optimal impingement distance was determined for both density ratios (isodensity and light jets). The use of PIV induced the design of an highly optical accessible new device. Different levels of confinement were investigated: free jets, confined jets, impinging jets and confined impinging jets (burner like configurations). Two very different pulse delay times were necessary to get accurate measurements everywhere, due to high velocity gradients combined with a macroscopic visualisation zone. A comparison between FFT intercorrelation and a new method was performed. A better resolution is obtained in the zones of highest gradients. Experiments were conducted for low turbulent and laminar jets. Up to really near the impingement plate, the jet behaves as free jets.

REFERENCES

Baydar, E. (1999). "Confined impinging jet at low Reynolds numbers", Experimental Thermal and Fluid Science, 19, pp. 27-33.

Djeridane, T., Amielh, M., Anselmet, F. and Fulachier, L. (1996). "Velocity properties in the near-field region of axisymmetric variable density jets", Physics of Fluids, 8, pp. 1615-1630.

Durst, F., Melling A. and Whitelaw J.H. (1981). "Principles and practice of laser-Doppler anemometry", Academic Press, Second Edition.

Hart, D.P. (1996). "Sparse array image correlation", Developments in Laser Techniques and Fluid Mechanics, Springer Editors, Selected Papers from the 8th International Symposium, Lisbon, Portugal, 8-11 July, pp. 53-74.

Hill, B.J. (1972). "Measurements of local entrainment rate in the initial region of axisymmetric turbulent air jets", Journal of Fluid Mechanics, 51, pp. 773-779.

Jones, H.R.N. (1989). "The application of combustion principles to domestic gas burner design", British Gas, E & F.N. Spon Editors.

Pagé, J. (1998). "Contribution à l'étude des jets turbulents axisymétriques à masse volumique variable", Thèse de l'Université d'Orléans, France.

Pitts, W.M. (1991). "Reynolds number effects on the mixing behavior of axisymmetric turbulent jets", Experiments in Fluids, 11, pp. 135-141.

Ricou, F.P. and Spalding, D.B. (1961). "Measurements of entrainment by axisymmetrical turbulent jets", Journal of Fluid Mechanics, 11, pp. 21-32.

ACKNOWLEDGEMENTS

The authors of this study acknowledge the Cooking Department of the Brandt company, the Conseil Régional Centre and the CNRS for their financial support. They are also grateful to the TSI company to have placed the last software version at their disposal, and to the LME and GREMI laboratories in Orléans for renting the LIF components.